Direct conversion of ethane to oxygenates, ethylene, and hydrogen in a non-catalytic biphasic plasma microreactor

Fabio Cameli,[1] Panagiotis Dimitrakellis,[1,2] and Dionisios G. Vlachos[1,2]

[1] *Department of Chemical and Biomolecular Engineering, University of Delaware, 150 Academy St., Newark, Delaware 19716, USA*

[2] *Catalysis Center for Energy Innovation, RAPID Manufacturing Institute, Delaware Energy Institute (DEI), 221 Academy St., Newark, Delaware 19716, USA*

Keywords:

Gas-to-liquid transformation, liquid fuels, hydrogen, electrification, modular reactors, non-thermal plasma

Abstract

We selectively upgrade ethane (C_2H_6) to ethanol (C_2H_5OH), methanol (CH_3OH), and acetic acid (CH_3COOH) in a catalyst-free, continuous, argon/water biphasic plasma microreactor. The water (H_2O) evaporates and electron-dissociates into $OH^{\cdot}$ radicals. $OH^{\cdot}$ recombines with alkyl radicals, produced via electron dissociation of ethane, to generate the oxygenates that absorb into H_2O. A plasma-assisted path, reminiscent of the low-temperature thermocatalytic ethane steam reforming, leads to significant H_2 co-production. The gaseous stream also comprises CO_2 and C_2H_4. Up to 1.3 and 1 μmol min^{-1} of liquid C_2H_5OH and CH_3OH are attained. Compared to CO_2-assisted ethane plasma conversion, which produces many oxygenates with low selectivity, the carbon selectivity can range from >70% to C_2H_5OH, CH_3OH, and CH_3COOH to 60% C_2H_4. The low carbon footprint, electrified, modular, intensified process using a reactive evaporation and separation plasma could pave the way for the valorization of underutilized shale gas resources in remote areas.

Ethane (C_2H_6) makes up to 10% of shale gas, depending on the source, and the large availability of shale gas makes its decentralized conversion, e.g., from flare gas, very attractive.[1, 2] Ethylene (C_2H_4) and its oxygenates, such as ethanol (C_2H_5OH), ethylene glycol (CH_2OHCH_2OH), ethylene oxide (C_2H_4O), and acetic acid (CH_3COOH), are essential C_2H_6 derivatives of significant market value.

The production of C_2H_4 via C_2H_6 dehydrogenation has been in the spotlight over the past decade as an alternative to the currently employed naphtha cracking. Thermo-catalytic processes dehydrogenate C_2H_6 above 550 °C with modest conversions.[3-5] The process suffers from equilibrium limitations. The catalysts coke and deactivate severely. Importantly, the dehydrogenation of small alkanes is highly endothermic, making C_2H_4 and propylene production the highest-emitting chemical processes next to ammonia. Electrification of C_2H_6 conversion is critical to decarbonizing the chemical industry. The direct catalytic production of oxygenates, such as C_2H_5OH, from C_2H_6, is even less straightforward due to the overoxidation to CO_2 when oxygen is used as a co-reagent. In the limited literature, N_2O is the most commonly employed oxidizing agent.[6-8] Chemical looping[7] and recycling[9] can increase productivity and stabilize the catalyst but are complex processes. A two-step conversion of C_2H_6 to C_2H_4 and then hydration to C_2H_5OH still suffers from the obstacles of C_2H_4 production.

A main hurdle in the activation of C_2H_6 lies in the high stability of the C-H bond that requires high energy input. Non-thermal atmospheric plasma (NTAP) is a low-energy, low-carbon footprint technology.[10, 11] A non-thermal plasma discharge, where the gas temperature is well below the electrons temperature, can activate small stable molecules like CH_4,[12-14] CO_2,[15-17] and N_2,[18-21]. Plasma-assisted activation of C_2H_6 has rarely been reported[22-24]; only one interesting study produced a mix of oxygenated species alongside light hydrocarbons via the dry reforming of C_2H_6 (C_2H_6+CO_2 cofed, with CO_2 as a soft oxidant).[25] Formaldehyde was the target of another study of dry reforming of C_2H_6[26] but the selectivity was low (i.e., below 12%). Packed-bed Dielectric Barrier Discharge (DBD) reactors are commonly employed to make gas-phase products. External cooling H_2O provided liquid oxygenates during the dry methane reforming.[27] Similarly, H_2O in the plasma zone can promote hydrocarbon oxidation[28, 29] or remove condensable oxygenates.[30] A general challenge in all plasma processes is that the products are also prone to dissociation in the plasma zone, limiting the maximum achievable productivity.

Herein, we introduce a simple, electrified system to produce oxygenates, namely a plasma biphasic microreactor[31] that uses slugs of liquid H_2O in a continuous gas stream of Argon (Ar) and C_2H_6. The microreactor allows for precise control of the slugs and the gas flow patterns, high interfacial area to enable the transfer of compounds from one phase to the next, and fast mass transfer between phases.[32] In addition, the system can be scaled out to maintain its performance. The two phases are intrinsically

separated, making product (gas and liquid) recovery easier. Even at low temperatures, a significant fraction of H_2O is present in the gas phase, due to evaporation. We hypothesize that H_2O vapor dissociation could form reactive oxygen species, such as $OH^{\cdot}$ and H_2O_2[31], that can partially oxidize C_2H_6. The desired overall reaction is R1. C_2H_6 dissociation followed by oxidation leads to the overall reaction R2.

$$\text{Plasma} - \text{induced ethane partial oxidation overall reactions:}$$

$$C_2H_6 + H_2O \rightarrow C_2H_5OH + H_2 \qquad (R1)$$

$$C_2H_6 + 2H_2O \rightarrow 2CH_3OH + H_2 \qquad (R2)$$

The products, CH_3OH and C_2H_5OH, can absorb into the aqueous phase and become protected from dissociation by the plasma allowing their concentration to increase with residence time. The microreactor operates as a reactive absorption unit where the H_2O serves the role of the oxidizer and the absorber. This scheme can also yield significant fractions of gaseous H_2 that can be stored or used for power generation and upgrading fuels, biomass, and plastics. Electrified H_2 production from low-carbon feedstocks is one of the pillars of the Hydrogen Earth shot.[33] We hypothesize that such a microreactor could enable the simultaneous production of liquid oxygenates and valuable gaseous products.

Our plasma microreactor consists of a coaxial DBD with a spiral tubular reactor through which liquid slugs flow in a continuous gas stream (Figure S1). The electrodes and tube lengths were adjusted to tune the residence time in the plasma. A gas mixture of Ar / C_2H_6 and liquid H_2O were cofed, and the plasma was ignited and sustained by a sinusoidal power supply. Gas chromatography was employed to analyze the liquid and gas phase composition. All experiments were run in triplicates, and error bars reflect the standard deviation. We exploit the role of operating parameters (applied voltage, C_2H_6 feed concentration, and liquid flow rate) on C_2H_6 conversion and product distribution. Plasma characterization via OES analysis was not possible due to noisy baseline caused by C_2H_6 in the gas discharge. No resolved peaks for N_2 or OH could be detected.

Figure 1a shows the strong correlation of the C_2H_6 conversion to the plasma dissipated power that, in turn, is controlled by varying the voltage (SI, eq. S3). The conversion increases sixfold by doubling the power, indicating the nonlinear nature of the process. Notably, the process is very selective: up to ~60% of the carbon ends up in oxygenates in the liquid phase, with the remaining carbon in the gas phase. Lower power leads mainly to C_2H_5OH and a smaller fraction of CH_3OH in the aqueous phase. CH_3COOH is detected only at the highest power, likely from the partial oxidation of ethanol. GCMS analysis also indicates traces

of CH_2OHCH_2OH and acetaldehyde (CH_3CHO) at the highest power level (at 9 kV), albeit with concentrations below the detection limit of the FID-GC used for product quantification. Carbon balance is above 90% for most experiments (Table S1). The higher degree of oxidation at higher power also corroborates with the rising CO_2 fraction in the gas.

H_2O_2 was not detected in the aqueous stream, likely due to the favorable gas-phase recombination of $OH^{\cdot}$ with alkyl radicals leading to alcohols ($R^{\cdot}+OH^{\cdot} \rightarrow ROH$), or its rapid consumption in liquid phase reactions. Liquid H_2O_2 could facilitate further oxidation of the absorbed oxygenates. An exhaustive list of the electron impact dissociation reactions and the non-activated radical recombination reactions that result in the overall reactions R1 and R2 is reported in the SI (Table S2-S5). Increased power enhances almost linearly the production rate of all products (Figure 1b). Increasing $OH^{\cdot}$ production via H_2O dissociation at high power leads to higher selectivity of the liquid oxygenates (Figure 1a).

The distribution of gaseous products is somewhat unexpected. The primary product is H_2 at a stoichiometry much higher than that of reactions R1 and R2. Gas-phase activation of C_2H_6 by the plasma leads to ethylene (C_2H_4) by electron impact dissociation, as expected, whose concentration also correlates positively with the power, albeit less than other species.

$$\text{Ethane dehydrogenation: } C_2H_6 \rightarrow C_2H_4 + H_2 \qquad (R3)$$

C_2H_4 also undergoes plasma-induced dissociation, and thereby, its selectivity drops at increasing power (Figure 1a). C_2H_6 dehydrogenation is potentially responsible for some of the H_2 via $2H^{\cdot} \rightarrow H_2$. We observe no C_2H_2 or larger hydrocarbons. The presence of H_2O vapor quenches these pathways. CO_2, the complete combustion product, is also seen in the gas phase. The selectivity of carbon-based products is up to 75% at high power. The CO_2 formation reflects plasma-induced steam reforming of C_2H_6 with a stoichiometry of:

$$\text{Observed plasma} - \text{induced ethane steam reforming: } C_2H_6 + 4H_2O \rightarrow 2CO_2 + 7H_2 \qquad (R4)$$

The rest of the detected H_2 must derive from H_2O dissociation which proved to be substantial in a Helium-H_2O configuration.[31]

Comparison to the thermochemical steam reforming of C_2H_6 at high temperatures (~900 ^{o}C) is instructive. It leads to syngas, where the water-gas shift (WGS) reaction contributes only slightly. The WGS's exothermic and equilibrium-limited nature marginalizes its effect on H_2 production at high

reforming temperatures. To overcome equilibrium limitations, the WGS reaction is typically run at lower temperatures in two stages. The thermally driven reactions are:

$$\text{Ethane steam reforming: } C_2H_6 + 2H_2O \rightarrow 2CO + 5H_2 \quad (R5)$$

$$\text{Water} - \text{gas shift (WGS): } CO + H_2O \rightarrow CO_2 + H_2 \quad (R6)$$

In contrast to the thermochemical process operating at high temperatures, the non-equilibrium, low-temperature plasma leads to CO_2 without producing CO, promoting H_2 production as depicted in R4. In essence, the low temperature of the DBD plasma could be thought of as driving the WGS reaction to the right. Effectively, this tandem process combines C_2H_6 steam reforming with the complete conversion of the WGS reaction. Consequently, the plasma process produces a significant fraction of H_2. Importantly, Joule heating does not play a central role in the plasma process as the liquid temperature never increases by more than 5 °C (i.e., 21 to 26 °C).

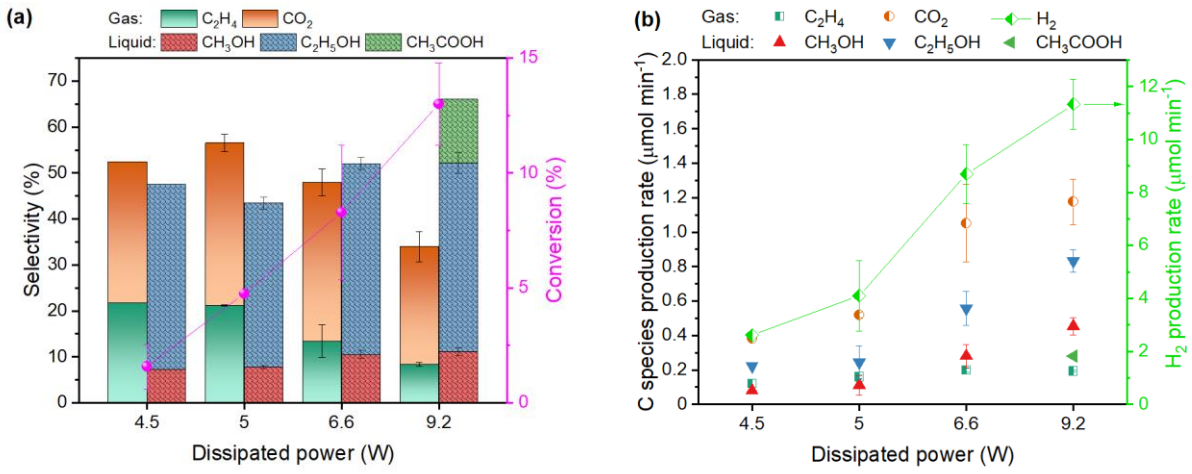

Figure 1. (a) C_2H_6 conversion and carbon-based product selectivity vs. dissipated power. (b) Production rate of gas (half symbols) and liquid (solid symbols) products vs. dissipated power. C_2H_6 mass flow: 98 µmol min^{-1}. Total gas flow rate: 300 sccm (1% C_2H_6 in Ar); liquid flow rate: 0.2 mL min^{-1}.

Figure 2a shows the C_2H_6 conversion upon increasing the C_2H_6 feed composition at constant applied voltage (Figure S2). The drop in conversion is due to the lower power channeled into the discharge (Figure S3). Consequently, the selectivity and production rate of all oxygenates decreases due to producing less $OH^{\cdot}$ (Figure 2a-b). CH_3COOH is observed only at C_2H_6 concentrations lower than 2%, and the CO_2 production rate increases more than fourfold when decreasing the C_2H_6 mole fraction from 2 to 0.8%. The

lower concentration of $OH^{\cdot}$ at lower power leaves behind a higher concentration of C_2H_4 that also undergoes electron-impact dissociation and oxidation, similarly to C_2H_6; the steady rise in C_2H_4 selectivity (up to 59%) and production rate in Figure 2a-b is owed to milder oxidation conditions (less CO_2 is formed). Moreover, decreasing the power reduces the H_2O dissociation and the H_2 production. This pathway dominates over C_2H_6 dehydrogenation as the H_2 production rate still drops (Figure 2b) even when higher amounts of C_2H_6 are converted in absolute value (Figure 2a).

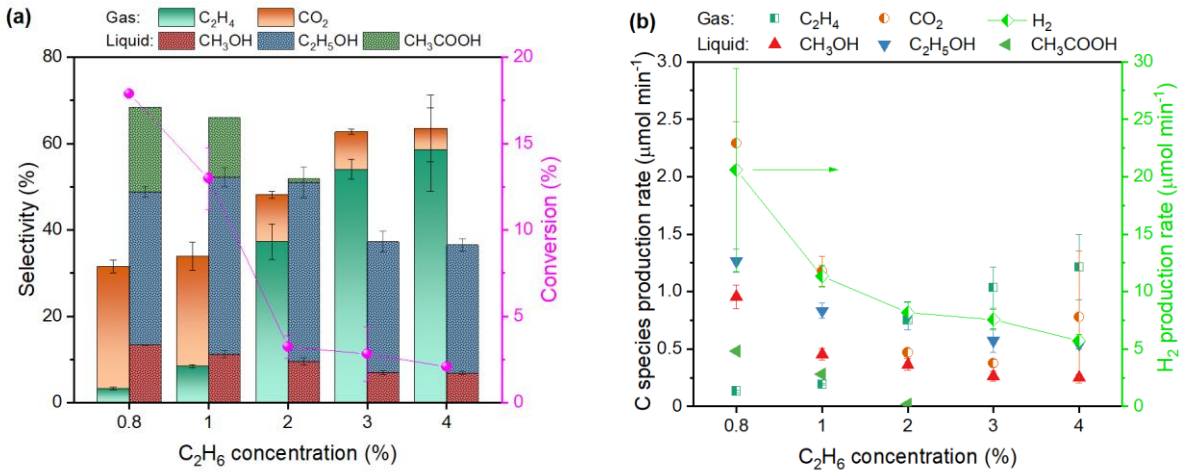

Figure 2. (a) C_2H_6 conversion and carbon-based selectivity to products vs. C_2H_6 feed composition. (b) Production rate of gas (half symbols) and liquid (solid symbols) products vs. C_2H_6 feed composition. Applied voltage: 9 kV. Gas flow rate: 300 sccm, liquid flow rate: 0.2 mL min^{-1}.

Aside from controlling the typical plasma knobs, the production of $OH^{\cdot}$ is affected by the fluid dynamics of the system. Liquid H_2O sources $OH^{\cdot}$ via desorption followed by dissociation in the plasma. Decreasing the liquid flow rate at a constant gas flow rate at first enhances the interfacial area and mass transfer between phases and improves C_2H_6 conversion. We previously demonstrated how a high gas-liquid interfacial area favors the absorption of $OH^{\cdot}$ into the liquid phase. Thereby, the higher selectivity to liquid oxygenates (Figure 3a) at a low liquid flow rate must be ascribed to the higher interfacial area. Contrariwise, a lower interfacial area promotes gas-phase oxidation and higher selectivity of CO_2 (Figure 3a). Nonetheless, the production rates of oxygenates are directly linked to the liquid flow rate: C_2H_5OH and CH_3OH productivity (SI, eq. S1) exhibits a maximum between 0.2 and 0.3 mL min^{-1}, above which the slow oxidation outweighs the benefit of the increased flow rate (Figure 3b). Interestingly, CH_3COOH is observed only at lower liquid flow rates. Its consumption at higher flow rates is partially compensated by an increase in C_2H_5OH production rate, suggesting that CH_3COOH is likely generated from the partial

oxidation of C_2H_5OH. H_2 production drops significantly only at the highest liquid flow rates due to the lower interfacial area that hinders H_2O evaporation and its subsequent dissociation.

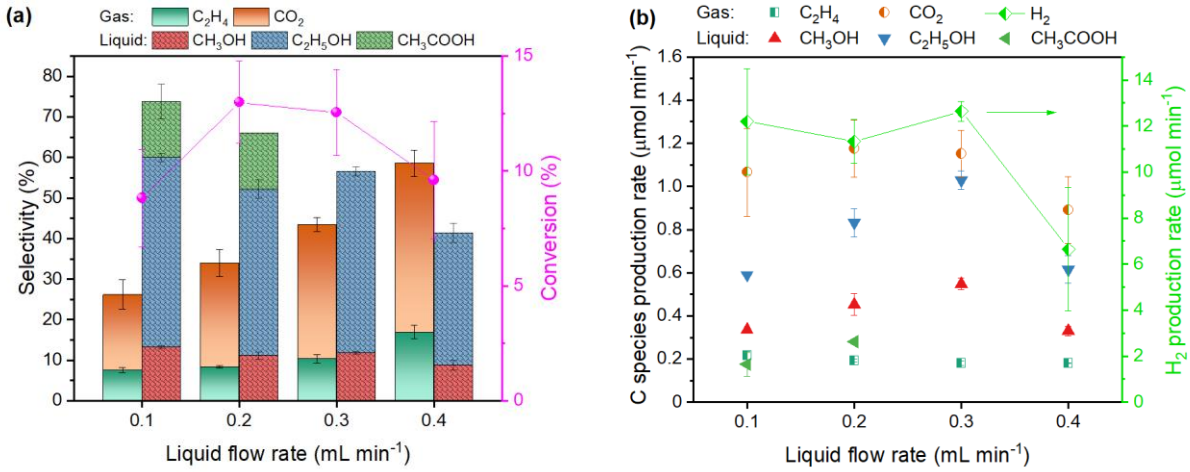

Figure 3. (a) C_2H_6 conversion and selectivity vs. the liquid H_2O flow rate. (b) Production rate of gas (half symbols) and liquid (solid symbols) products vs. liquid H_2O flow rate. C_2H_6 mass flow: 98 μmol min^{-1}. Applied voltage: 9 kV. Total gas flow rate: 300 sccm (1% C_2H_6 in Ar).

The fundamental pathways of the overall chemistry are also fascinating. Electron-impact dissociation reactions dominate cold DBD plasmas.[34] In the absence of an oxidizer (a dry plasma), C_2H_6 is converted to stable hydrocarbons, mainly C_2H_4 and C_2H_2, and to alkyl (C_2H_5 and CH_3) and H radicals that recombine with each other to form small fractions of methane (CH_4) and C_3 and C_4 hydrocarbons. The overall key reactions expected, based on the branching ratios (BR),[35] are

$$\text{Ethylene formation: } C_2H_6 \rightarrow C_2H_4 + H_2, BR = 0.46 \quad (R7)$$

$$\text{Acetylene formation: } C_2H_6 \rightarrow C_2H_2 + 2H_2, BR = 0.11 \quad (R8)$$

The reactions forming radicals are

$$\text{Ethyl formation: } C_2H_6 \rightarrow C_2H_5^{\cdot} + H^{\cdot}, BR = 0.24 \quad (R9)$$

$$\text{Methyl formation: } C_2H_6 \rightarrow 2CH_3^{\cdot}, BR = 0.08 \quad (R10)$$

Given the above stoichiometry, the ratio of H_2 to C_2H_4 is expected to be between 1 and 2. A fraction of the H_2 is used up to saturate alkyl radicals into stable hydrocarbons, e.g., CH_4 and C_3H_8. Based on the BRs, C_2H_4 is expected to be 4x and 2x as much as C_2H_2 and $C_2H_5^{\cdot}$, respectively, by the first electron impact

dissociation, with the majority of $C_2H_5^{\cdot}$ converting to C_2H_4 upon a second electron impact dissociation reaction, $C_2H_5^{\cdot} \rightarrow C_2H_4+H^{\cdot}$.

Unlike the dry ethane plasma chemistry, in our system H_2O evaporates from the liquid to the gas phase where the H_2O molecules are dissociated into $OH^{\cdot}+H^{\cdot}$ through electron impact reactions (threshold energy: 7 eV).[36] In our system the H_2O fraction in the plasma is high and other routes to $OH^{\cdot}$ are also possible in an Ar atmosphere.[37] Although the main dissociative channel for C_2H_6 leads to C_2H_4 due to the low threshold energy (4 eV), electron impact also yields $CH_3^{\cdot}$ and $C_2H_5^{\cdot}$ radicals (threshold energies of 6.4 and 7.5 eV, respectively)[35]. Radical recombination is a favorable oxidation route due to these reactions being non-activated (Table S5).[29] Hence, the recombination of $OH^{\cdot}$ and alkyl radicals causes the first oxidation, e.g., $R^{\cdot}+OH^{\cdot} \rightarrow ROH$. In our case, this reaction leads to the formation of C_2H_5OH and CH_3OH:

$$\text{Ethanol formation: } C_2H_5^{\cdot} + OH^{\cdot} \rightarrow C_2H_5OH \qquad (R11)$$

$$\text{Methanol formation: } CH_3^{\cdot} + OH^{\cdot} \rightarrow CH_3OH \qquad (R12)$$

$H^{\cdot}$ abstraction from the alkyl radical via $OH^{\cdot}$ forms alkenes, e.g., $CH_2CH_3^{\cdot}+OH^{\cdot} \rightarrow C_2H_4+H_2O$. Ketones and aldehydes are generated in subsequent oxidations, $RCH_2OH^{\cdot}+2OH^{\cdot} \rightarrow RCHO+2H_2O$ and can further be oxidized to acids. $OH^{\cdot}$ radicals are the most effective oxidizers: they promote $H^{\cdot}$ abstraction from alcohols to form carbonyl compounds and they add to the C=O bond leading to the formation of carboxylic groups.

Given the large fractions of oxygenates and the relatively small fractions of alkyl radicals expected based on the branching ratios, the data indicates that direct $H^{\cdot}$ abstraction from C_2H_6 may be possible, $CH_3CH_3+OH^{\cdot} \rightarrow C_2H_5^{\cdot}+H_2O$; $CH_2CH_3^{\cdot}+OH^{\cdot} \rightarrow C_2H_4+H_2O$. $H^{\cdot}$ abstraction by $OH^{\cdot}$ is exothermic and proceeds with a low energy barrier. Such reactions, proposed by Locke and co-workers based on quantum mechanical calculations,[29] create additional channels to both oxygenates and alkenes beyond the electron impact dissociation reactions. A possible reaction scheme for producing oxygenates is drawn in Figure 4.

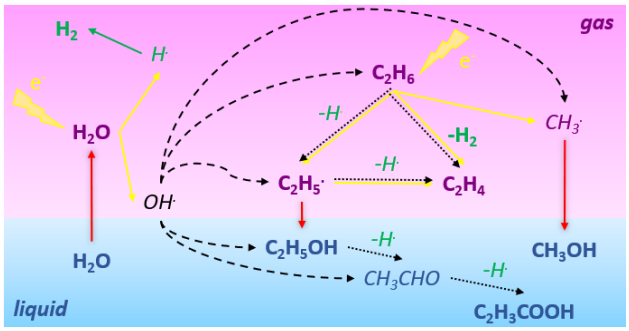

Figure 4. Simplified reaction scheme for the H_2O-assisted plasma-activation of C_2H_6. The yellow and black arrows represent electron impact and oxidation reactions, respectively. The red arrows indicate mass transfer between phases. The green arrows are related to radical recombination. Bold font is used for stable measured species, italic font indicates intermediate species.

The plasma-assisted dry C_2H_6 reforming generates several more oxygenates with a total selectivity below 5% and a selectivity to CO and olefins of 10 to 30%,[25] rendering product separation challenging. In this regard, catalyst development in CO_2-assisted chemistry is essential and expected to play a significant role in future studies. In comparison, the water-assisted process is more selective to oxygenates without a catalyst. CH_3OH and C_2H_5OH can be separated from water by distillation and used in various applications, including blending them into fuels to reduce soot and knocking.[38] Membrane technology is already used to purify H_2 from natural gas streams and remove CO_2 impurities.[39, 40] In the bigger picture, both mild oxidant-assisted processes unlock new opportunities for chemical production.

The energy cost of each product of all experimental sets is reported in Table S6. Whilst these values are much higher than industrial state of the art single-product manufacturing, they represent a promising starting point for a non-optimized process that simultaneously produces value-added products in separate streams with low input power (i.e., max 10 W).

In summary, a biphasic plasma microreactor was employed to produce oxygenates from gaseous C_2H_6 and liquid H_2O. H_2O serves a dual role. As an oxidizer, it provides H_2O vapor that dissociates in the plasma to create $OH^{\cdot}$ in situ and drive the oxidation. As an absorber, it removes the oxygenates from the plasma to avoid their plasma-driven degradation. This integrated (evaporator, reactor, and absorber) unit produces significantly fewer oxygenates than gas-phase-only CO_2-assisted CH_4 and C_2H_6 conversion. The biphasic plasma microreactor is catalyst-free, avoiding catalyst cost and deactivation challenges. It attains C_2H_5OH and CH_3OH liquid phase productivity of ~1.3 and 1 µmol min^{-1}, respectively, about 7x that of the packed-bed plasma reactor of C_2H_6 dry reforming (0.3 µmol min^{-1} productivity of both C_2H_5OH and CH_3OH in the gas mixture and 70% higher power).[25] The direct conversion of hydrocarbons to oxygenates has been a long-standing goal, and this process achieves this. More detailed comparisons between single phase and biphasic and catalytic and non-catalytic systems are necessary in future work to find the best

use of plasma reactors. Modeling would also be welcome. The biphasic configuration separates the oxygenates-rich liquid phase from the gas phase containing H_2 and C_2H_4 but includes water as an additional phase. The system is tunable by controlling the power, C_2H_6 concentration, and liquid flow rate. We propose that reactive absorption (as done here) or adsorption (using a solid sorbent) is a potentially transformative technology to overcome the selectivity challenges of gas-phase plasma reactors, without a catalyst. The reactive separation approach proposed here opens new possibilities for selective catalyst-free plasma processes.

Supporting Information

Experimental procedure. Electrical measurements. Carbon balance. Plasma reactions.

Acknowledgements

This work was supported from Department of Energy's Office of Energy Efficient and Renewable Energy's Advanced Manufacturing Office under Award Number DE-EE0007888-8.3. The Delaware Energy Institute gratefully acknowledges the support and partnership of the State of Delaware toward the RAPID projects.

References

(1) Porosoff, M. D.; Myint, M. N. Z.; Kattel, S.; Xie, Z.; Gomez, E.; Liu, P.; Chen, J. G. Identifying Different Types of Catalysts for CO2 Reduction by Ethane through Dry Reforming and Oxidative Dehydrogenation. *Angewandte Chemie - International Edition* **2015**, *54* (51), 15501-15505. DOI: 10.1002/anie.201508128.
(2) Kim, S.; Oh, S. Impact of US Shale Gas on the Vertical and Horizontal Dynamics of Ethylene Price. *Energies* **2020**, *13* (17). DOI: 10.3390/EN13174479.
(3) Dai, Y.; Gao, X.; Wang, Q.; Wan, X.; Zhou, C.; Yang, Y. Recent progress in heterogeneous metal and metal oxide catalysts for direct dehydrogenation of ethane and propane. *Chemical Society Reviews* **2021**, *50* (9), 5590-5630. DOI: 10.1039/d0cs01260b.
(4) Wang, C.; Yang, B.; Gu, Q.; Han, Y.; Tian, M.; Su, Y.; Pan, X.; Kang, Y.; Huang, C.; Liu, H.; et al. Near 100% ethene selectivity achieved by tailoring dual active sites to isolate dehydrogenation and oxidation. *Nature Communications* **2021**, *12* (1), 1-8. DOI: 10.1038/s41467-021-25782-2.
(5) Wu, L.; Fu, Z.; Ren, Z.; Wei, J.; Gao, X.; Tan, L.; Tang, Y. Enhanced Catalytic Performance of Fe-containing HZSM-5 for Ethane Non-Oxidative Dehydrogenation via Hydrothermal Post-Treatment. *ChemCatChem* **2021**, *13* (18), 4019-4028. DOI: 10.1002/cctc.202100752.
(6) Xiao, D. J.; Bloch, E. D.; Mason, J. A.; Queen, W. L.; Hudson, M. R.; Planas, N.; Borycz, J.; Dzubak, A. L.; Verma, P.; Lee, K.; et al. Oxidation of ethane to ethanol by N2 O in a metal-organic framework with coordinatively unsaturated iron(II) sites. *Nature Chemistry* **2014**, *6* (7), 590-595. DOI: 10.1038/nchem.1956.

(7) He, X.; Li, Z.; Hu, H.; Chen, J.; Zeng, L.; Zhang, J.; Lin, W.; Wang, C. Chemical looping conversion of ethane to ethanol via photo-assisted nitration of ethane. *Cell Reports Physical Science* **2021**, *2* (7), 100481. DOI: https://doi.org/10.1016/j.xcrp.2021.100481.
(8) Verma, P.; Vogiatzis, K. D.; Planas, N.; Borycz, J.; Xiao, D. J.; Long, J. R.; Gagliardi, L.; Truhlar, D. G. Mechanism of oxidation of ethane to ethanol at Iron(IV)-oxo sites in magnesium-diluted Fe2(dobdc). *Journal of the American Chemical Society* **2015**, *137* (17), 5770-5781. DOI: 10.1021/jacs.5b00382.
(9) Jin, R.; Peng, M.; Li, A.; Deng, Y.; Jia, Z.; Huang, F.; Ling, Y.; Yang, F.; Fu, H.; Xie, J.; et al. Low Temperature Oxidation of Ethane to Oxygenates by Oxygen over Iridium-Cluster Catalysts. *Journal of the American Chemical Society* **2019**, *141* (48), 18921-18925. DOI: 10.1021/jacs.9b06986.
(10) Weltmann, K. D.; Kolb, J. F.; Holub, M.; Uhrlandt, D.; Šimek, M.; Ostrikov, K.; Hamaguchi, S.; Cvelbar, U.; Černák, M.; Locke, B.; et al. The future for plasma science and technology. *Plasma Processes and Polymers* **2019**, *16* (1), 1-29. DOI: 10.1002/ppap.201800118.
(11) Nguyen, D. K.; Dimitrakellis, P.; Talley, M. R.; O'Dea, R. M.; Epps, T. H., III; Watson, M. P.; Vlachos, D. G. Oxidative Functionalization of Long-Chain Liquid Alkanes by Pulsed Plasma Discharges at Atmospheric Pressure. *ACS Sustainable Chemistry & Engineering* **2022**. DOI: 10.1021/acssuschemeng.2c04269.
(12) Delikonstantis, E.; Scapinello, M.; Van Geenhoven, O.; Stefanidis, G. D. Nanosecond pulsed discharge-driven non-oxidative methane coupling in a plate-to-plate electrode configuration plasma reactor. *Chemical Engineering Journal* **2020**, *380*, 122477-122477. DOI: https://doi.org/10.1016/j.cej.2019.122477.
(13) Delikonstantis, E.; Scapinello, M.; Stefanidis, G. D. Low energy cost conversion of methane to ethylene in a hybrid plasma-catalytic reactor system. *Fuel Processing Technology* **2018**, *176*, 33-42. DOI: https://doi.org/10.1016/j.fuproc.2018.03.011.
(14) Puliyalil, H.; Jurković, D. L.; Dasireddy, V. D. B. C.; Likozar, B. A review of plasma-assisted catalytic conversion of gaseous carbon dioxide and methane into value-added platform chemicals and fuels. *RSC advances* **2018**, *8* (48), 27481-27508.
(15) Mei, D.; Zhu, X.; Wu, C.; Ashford, B.; Williams, P. T.; Tu, X. Plasma-photocatalytic conversion of CO2 at low temperatures: Understanding the synergistic effect of plasma-catalysis. *Applied Catalysis B: Environmental* **2016**, *182*, 525-532. DOI: https://doi.org/10.1016/j.apcatb.2015.09.052.
(16) Bogaerts, A.; Centi, G. Plasma Technology for CO2 Conversion: A Personal Perspective on Prospects and Gaps. *Frontiers in Energy Research* **2020**, *8*, Review. DOI: 10.3389/fenrg.2020.00111.
(17) Delikonstantis, E.; Scapinello, M.; Singh, V.; Poelman, H.; Montesano, C.; Martini, L. M.; Tosi, P.; Marin, G. B.; Van Geem, K. M.; Galvita, V. V.; et al. Exceeding Equilibrium CO2Conversion by Plasma-Assisted Chemical Looping. *ACS Energy Letters* **2022**, 1896-1902. DOI: 10.1021/acsenergylett.2c00632.
(18) Kelly, S.; Bogaerts, A. Nitrogen fixation in an electrode-free microwave plasma. *Joule* **2021**, *5* (11), 3006-3030. DOI: https://doi.org/10.1016/j.joule.2021.09.009.
(19) Winter, L. R.; Chen, J. G. N2 Fixation by Plasma-Activated Processes. *Joule* **2021**, *5* (2), 300-315. DOI: https://doi.org/10.1016/j.joule.2020.11.009.
(20) Hollevoet, L.; Jardali, F.; Gorbanev, Y.; Creel, J.; Bogaerts, A.; Martens, J. A. Towards Green Ammonia Synthesis through Plasma-Driven Nitrogen Oxidation and Catalytic Reduction. *Angewandte Chemie International Edition* **2020**, *59* (52), 23825-23829. DOI: https://doi.org/10.1002/anie.202011676.
(21) Gromov, M.; Kamarinopoulou, N.; De Geyter, N.; Morent, R.; Snyders, R.; Vlachos, D. G.; Dimitrakellis, P.; Nikiforov, A. Plasma-assisted nitrogen fixation: the effect of water presence. *Green Chemistry* **2022**, 10.1039/D2GC03063B. DOI: 10.1039/D2GC03063B.
(22) Zhang, X.; Zhu, A.; Li, X.; Gong, W. Oxidative dehydrogenation of ethane with CO2 over catalyst under pulse corona plasma. *Catalysis Today* **2004**, *89* (1-2), 97-102. DOI: 10.1016/j.cattod.2003.11.015.
(23) Trionfetti, C.; Ağiral, A.; Gardeniers, H. J. G. E.; Lefferts, L.; Seshan, K. Alkane activation at ambient temperatures: Unusual selectivities, C-C, C-H bond scission versus C-C bond coupling. *ChemPhysChem* **2008**, *9* (4), 533-537. DOI: 10.1002/cphc.200700757.

(24) Jensen, R. J.; Bell, A. T.; Soong, D. S. Plasma polymerization of ethane. I. Experimental studies of effluent gas composition and polymer deposition rates. *Plasma Chemistry and Plasma Processing* **1983**, *3* (2), 139-161. DOI: 10.1007/BF00566018.
(25) Biswas, A. N.; Winter, L. R.; Loenders, B.; Xie, Z.; Bogaerts, A.; Chen, J. G. Oxygenate Production from Plasma-Activated Reaction of CO2and Ethane. *ACS Energy Letters* **2022**, *7* (1), 236-241. DOI: 10.1021/acsenergylett.1c02355.
(26) Gómez-Ramírez, A.; Rico, V. J.; Cotrino, J.; González-Elipe, A. R.; Lambert, R. M. Low temperature production of formaldehyde from carbon dioxide and ethane by plasma-Assisted catalysis in a ferroelectrically moderated dielectric barrier discharge reactor. *ACS Catalysis* **2014**, *4* (2), 402-408. DOI: 10.1021/cs4008528.
(27) Wang, Y.; Chen, Y.; Harding, J.; He, H.; Bogaerts, A.; Tu, X. Catalyst-free single-step plasma reforming of CH4 and CO2 to higher value oxygenates under ambient conditions. *Chemical Engineering Journal* **2022**, *450*. DOI: 10.1016/j.cej.2022.137860.
(28) Wandell, R. J.; Bresch, S.; Hsieh, K.; Alabugin, I. V.; Locke, B. R. Formation of Alcohols and Carbonyl Compounds From Hexane and Cyclohexane With Water in a Liquid Film Plasma Reactor. *IEEE Transactions on Plasma Science* **2014**, *42* (5), 1195-1205. DOI: 10.1109/tps.2014.2304183.
(29) Bresch, S.; Wandell, R.; Wang, H.; Alabugin, I.; Locke, B. R. Oxidized Derivatives of n-Hexane from a Water/Argon Continuous Flow Electrical Discharge Plasma Reactor. *Plasma Chemistry and Plasma Processing* **2015**, *36* (2), 553-584. DOI: 10.1007/s11090-015-9686-x.
(30) Ağıral, A.; Nozaki, T.; Nakase, M.; Yuzawa, S.; Okazaki, K.; Gardeniers, J. G. E. Gas-to-liquids process using multi-phase flow, non-thermal plasma microreactor. *Chemical Engineering Journal* **2011**, *167* (2), 560-566. DOI: https://doi.org/10.1016/j.cej.2010.10.050.
(31) Cameli, F.; Dimitrakellis, P.; Chen, T.-y.; Vlachos, D. G. Modular Plasma Microreactor for Intensified Hydrogen Peroxide Production. *ACS Sustainable Chemistry and Engineering* **2022**. DOI: 10.1021/acssuschemeng.1c06973.
(32) Chen, T.-Y.; Hsiao, Y. W.; Baker-Fales, M.; Cameli, F.; Dimitrakellis, P.; Vlachos, D. G. Microflow chemistry and its electrification for sustainable chemical manufacturing. *Chemical Science* **2022**, *13* (36), 10644-10685, 10.1039/D2SC01684B. DOI: 10.1039/D2SC01684B.
(33) https://www.energy.gov/eere/fuelcells/hydrogen-shot (accessed.
(34) Heijkers, S.; Aghaei, M.; Bogaerts, A. Plasma-Based CH4 Conversion into Higher Hydrocarbons and H2: Modeling to Reveal the Reaction Mechanisms of Different Plasma Sources. *The Journal of Physical Chemistry C* **2020**, *124* (13), 7016-7030. DOI: 10.1021/acs.jpcc.0c00082.
(35) Janev, R. K.; Reiter, D. Collision processes of hydrocarbon species in hydrogen plasmas. Part 2. The ethane and propane families. *ChemInform* **2003**, *34* (37), no-no.
(36) Itikawa, Y.; Mason, N. Cross Sections for Electron Collisions with Water Molecules. *Journal of Physical and Chemical Reference Data* **2005**, *34* (1), 1-22. DOI: 10.1063/1.1799251 (acccessed 2022/11/17).
(37) Liu, D.; Sun, B.; Iza, F.; Xu, D.; Wang, X.; Rong, M.; Kong, M. G. Main species and chemical pathways in cold atmospheric-pressure Ar + H2O plasmas. *Plasma Sources Science and Technology* **2017**, *26* (4), 045009. DOI: 10.1088/1361-6595/aa5c22.
(38) Dong, Y.; Dai, C.; Lei, Z. Separation of the Methanol–Ethanol–Water Mixture Using Ionic Liquid. *Industrial & Engineering Chemistry Research* **2018**, *57* (32), 11167-11177. DOI: 10.1021/acs.iecr.8b01617.
(39) Luo, S.; Zhang, Q.; Zhu, L.; Lin, H.; Kazanowska, B. A.; Doherty, C. M.; Hill, A. J.; Gao, P.; Guo, R. Highly Selective and Permeable Microporous Polymer Membranes for Hydrogen Purification and CO2 Removal from Natural Gas. *Chemistry of Materials* **2018**, *30* (15), 5322-5332. DOI: 10.1021/acs.chemmater.8b02102.
(40) Lin, H.; He, Z.; Sun, Z.; Vu, J.; Ng, A.; Mohammed, M.; Kniep, J.; Merkel, T. C.; Wu, T.; Lambrecht, R. C. CO2-selective membranes for hydrogen production and CO2 capture – Part I: Membrane development. *Journal of Membrane Science* **2014**, *457*, 149-161. DOI: https://doi.org/10.1016/j.memsci.2014.01.020.

For Table of Contents Use Only

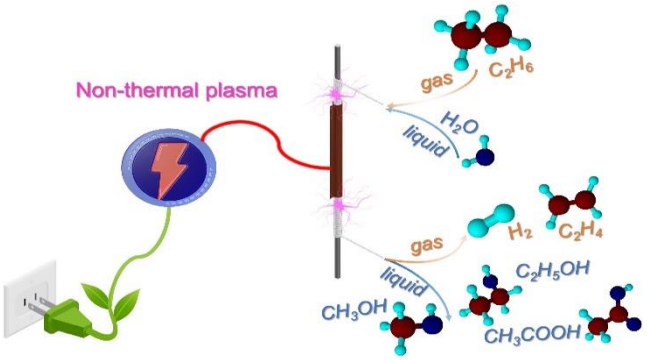

Modular, biphasic plasma reactor enables upgrading of underutilized gas streams into liquid fuels and hydrogen for electrified and decentralized chemical processing.